Journal of Photochemistry & Photobiology, B: Biology 240 (2023) 112652

Contents lists available at ScienceDirect

Journal of Photochemistry & Photobiology, B: Biology

journal homepage: www.elsevier.com/locate/jphotobiol

An indolizine squaraine-based water-soluble NIR dye for fluorescence imaging of multidrug-resistant bacteria and antibacterial/antibiofilm activity using the photothermal effect

Sanjay Singh [a], William E. Meador [b], Avijit Pramanik [a], Paresh Ray [a], Jared H. Delcamp [b,1,2], Yongfeng Zhao [a,*]

[a] Department of Chemistry, Physics & Atmospheric Sciences, Jackson State University, Jackson, MS 39217, United States of America
[b] Department of Chemistry and Biochemistry, University of Mississippi, University, MS 38677, United States of America

ARTICLE INFO

Keywords:
SO_3SQ
Near-infrared
Photothermal therapy
Antibacterial
Antibiofilm

ABSTRACT

The majority of nosocomial infections are caused by bacteria with antimicrobial resistance and the formation of biofilms, such as implant-related bacterial infections and sepsis. There is an urgent need to develop new strategies for early-stage screening, destruction of multidrug-resistant bacteria, and efficient inhibition of biofilms. Organic dyes that absorb and emit in the near-infrared (NIR) region are potentially non-invasive, high-resolution, and rapid biological imaging materials. In this study, a non-toxic and biocompatible indolizine squaraine dye with water-solubilizing sulfonate groups (SO_3SQ) is studied for bacterial imaging and photothermal therapy (PTT). PTT is efficient in eliminating microorganisms through local hyperthermia without the risk of developing drug-resistant bacteria. The optical properties of SO_3SQ are studied extensively in phosphate-buffered saline (PBS). UV–Vis–NIR absorption spectra analysis shows a strong absorption between 650 nm – 1000 nm. SO_3SQ allows for the wash-free fluorescence imaging of drug-resistant bacteria via NIR fluorescence imaging due to a "turn-on" fluorescence property of the dye when interacting with bacteria. Although SO_3SQ exhibits no toxicity against both Gram-positive bacteria and Gram-negative bacteria, the PTT property of SO_3SQ is efficient in killing bacteria as well as inhibiting and eradicating biofilms. PTT experiments demonstrate that SO_3SQ reduces 90% of cell viability in bacterial strains under NIR radiation with a minimum inhibition concentration (MIC_{90}) of >450 μg/mL. The PTT property of SO_3SQ can also inhibit biofilms (BIC_{90} = 1000–2000 μg/mL) and eradicate both preformed young and mature biofilms ($MBEC_{90}$ = 1500–2000 μg/mL) as observed by crystal violet assays.

1. Introduction

Bacterial infections, such as implant-related bacterial infections and sepsis, are major public health concerns that can cause fatal diseases. [1,2] Infectious diseases account for about 25% of all deaths each year, and in some developing countries this percentage is as high as 30–50%. [3] These infections are mostly caused by drug-resistant and biofilm-forming bacteria. [4] In particular, *Staphylococcus aureus* and *Escherichia coli* are the most common microorganisms for infections associated with foreign implants such as prosthetic joints, central venous catheters, cerebrospinal fluid shunts, intracardiac devices, heart valve prostheses, and vascular grafts. [5,6] Furthermore, the widespread overuse of antibiotics and the formation of biofilms worsens emerging severe global health problems from drug-resistant bacteria. [7,8] Genetic mutations, phenotypic changes, and the protection of the extracellular matrices in biofilms play an essential role in developing penetration resistance toward antibiotics, thus increasing antibiotic resistance. [9,10] Recently, the World Health Organization (WHO) has prioritized pathogens that are resistant to antibiotics, with *Streptococcus pneumonia, Escherichia coli, Salmonella typhi* and *Staphylococcus aureus* classified as critical and of high priority. [11] The Centers for Disease Control and Prevention (CDC) has also identified antibiotic-resistant bacteria as a severe threat

* Corresponding author.
E-mail address: yongfeng.zhao@jsums.edu (Y. Zhao).
[1] Present Address: Air Force Research Laboratory, Materials and Manufacturing Directorate (RXNC), 2230 Tenth Street B655, Wright-Patterson AFB, OH 45433, USA.
[2] Present Address: UES, Inc., 4401 Dayton Xenia Rd, Dayton, OH 45432, USA.

https://doi.org/10.1016/j.jphotobiol.2023.112652
Received 4 November 2022; Received in revised form 3 January 2023; Accepted 13 January 2023
Available online 18 January 2023
1011-1344/

to public health. [12] This rapidly escalating threat has raised an urgent need for early-stage detection and effective killing of pathogens that are highly antibiotic resistant and their biofilms. Ideally, the combination of imaging and treatment is particularly desired.

Traditional methods of identifying bacteria, such as culture and colony counting, are time-consuming and labor intensive. They often require a complex series of measurements and take weeks to obtain reliable results. [13] To overcome these problems, the development of fluorescent probes capable of identifying bacteria is of great attention. [14,15] Inorganic fluorescent probes, such as inorganic nanoparticles, quantum dots, and carbon-based nanoprobes, are widely used in bioimaging due to their high photothermal stabilities, strong absorptions, and excellent electron transfer capabilities. [16,17] However, they usually face the problem of long-term toxicity in the body. [18] Alternatively, fluorescent probes based on organic fluorescent dyes have been considered to be one of the most effective fluorescent tools for bacterial detection and imaging due to their high sensitivity [19,20] and selectivity [21,22]. In addition, small organic molecules can be quickly removed from the body. Their advantages include excellent biocompatibility, [23] ease of handling, [24] and ease of molecular structure modification. [25,26] Furthermore, as an effort to increase sensitivity, bacterial detection can be significantly improved by the introduction of organic dyes that turn on fluorescence while interacting with bacteria. [27,28] These switchable dyes have demonstrated many advantages for imaging bacteria, including low background signal generation, high specificity, and wash-free procedures.

Regarding bacterial eradication, chemotherapy and non-chemotherapy are the two major strategies for killing drug-resistant bacteria. [29] Chemotherapy employs multi-fold antibiotics, while nonchemotherapy takes advantage of photodynamic therapy (PDT) and photothermal therapy (PTT). [30] Because PTT kills bacteria by increasing the temperature around bacteria, PTT is a preferred strategy to kill bacteria as it does not develop drug resistance. Many materials have been developed and used as photothermal agents, including inorganic nanomaterials (based on Au, Ag, and CuS) and semiconductors (based on graphene and carbon nanotubes). [31–33] Although some progress has been made, superior photothermal agents with low toxicity remain to be developed for rapid and effective antimicrobial photothermal therapy. Desirably, organic materials have been shown to have high PTT efficiencies as well as low toxicities. [34–36] In recent years, near-infrared (NIR, 700–1000 nm) dyes have attracted increasing attention for imaging and therapeutic applications. [37] The NIR region is an ideal therapeutic window for in vivo applications due to minimized absorption, photo scattering, and autofluorescence of biomolecules and tissues in this region. As a promising antibacterial method, PTT has shown clear advantages in killing bacteria and destroying the biofilm structure. [35,38–40]

Squaraine dyes are a class of organic dyes with a central electron deficient four member ring within a resonance stabilized zwitterionic structures. [41] Due to their resonance zwitterionic properties and planar structures, squaraine dyes exhibit strong absorption and emission in the NIR region. [42] To increase the water solubility for biological applications, the introduction of sulfonate groups is a practical approach. [43,44] Squaraine dyes have been intensely studied for PDT. [45] Ramaiah and co-workers reported that halogenated squaraine dyes can efficiently generate singlet oxygen for PDT treatment while non-halogenated squaraine dyes exhibit negligible singlet oxygen generation. [46] These halogenated squaraine dyes demonstrated increased toxicity to both bacteria and mammalian cells upon excitation. Both brominated and iodinated squaraine dyes induce cytotoxic effects and DNA damage predominantly via singlet oxygen generation. [47] In vitro cytotoxicity studies of iodinated bisbenzothiazolium squaraine dyes with DLA live cells showed high cytotoxicity. [43] Although PDT treatment has been promising for some applications, hypoxic cellular microenvironments inherently compromise PDT efficacy. Thus, PTT is a good alternative in hypoxic scenarios.

In this work, an indolizine squaraine-based dye bearing sulfonate groups (SO_3SQ) is studied for the detection and killing of drug-resistant bacteria by PTT. *Escherichia coli* (*E. coli*) and Methicillin-resistant *Staphylococcus aureus* (MRSA) are used as model pathogens. The sensitivity of SO_3SQ for bacterial detection is exceptional as the dye exhibits strong turn-on fluorescence upon interacting directly with bacteria and minimal fluorescence in the background aqueous solution. At the same time, the dye can eliminate bacteria and biofilms by absorbing and converting NIR light into heat. SO_3SQ also has the potential for deep tissue penetration and low toxicity due to its absorption and emission in the NIR region. This study represents a novel study of the fluorescent dye SO_3SQ that allows for wash-free imaging and killing of drug-resistant bacteria under NIR radiation. The destruction of biofilms with SO_3SQ is also studied and demonstrated herein.

2. Materials and Method

SO_3SQ was synthesized as previously reported. [48] The chemical structure is shown in Fig. S1. Phosphate-buffered saline (PBS, 1×) is used as an isotonic solution consisting of NaCl (137 mM), KCl (2.7 mM), Na_2HPO_4 (10 mM), and KH_2PO_4 (1.8 mM). The pH is further adjusted to 7.4 by adding HCl/NaOH accordingly using a pH meter. Nutrient Agar (NA) and Nutrient Broth (NB) were purchased from Sigma-Aldrich (St Louis, MO).

2.1. Microorganism and Cultural Conditions

The Gram-negative bacterial strain *E. coli* and Gram-positive bacterial strain MRSA were employed in this study. These bacterial strains were cultured in Nutrient Broth (NB), at 37 °C in a shaker for 6 h at 150 rpm and then prepared in secondary cultures to obtain the cells in their exponential phase at 0.6–0.7 OD_{600}. The cells were pelleted by centrifugation at 1073 ×*g* for 10 min and then resuspended in 1 mL of NB media. The OD_{600} cells were then adjusted to 0.1 to maintain cell concentration up to 10^8 CFU/mL.

2.2. Characterization

The ^{1}H NMR spectra were recorded on a Bruker Ascend-400 (400 MHz) spectrometer and are reported in ppm using solvent as an internal standard. SO_3SQ was dissolved in PBS solutions at the various concentrations specified in the text. The absorbance was recorded using a UV–Vis–NIR absorption spectrophotometer (UV-2600, UV–Vis spectrophotometer, Shimadzu, Japan) to check the absorption of the dye from 200 nm – 1000 nm. Fluorescence spectroscopy was used to measure the emission of the dye with excitation wavelengths ranging from 600 to 800 nm. All emission data were obtained using a Horiba PTI fluorimeter (FluoroMax-4, Spectofluorometer, Horiba, Japan). The photothermal characteristics of the dye were studied using an 808 nm wavelength laser equipped with a thermal imaging camera.

2.3. Bacterial Imaging

Bacterial cultures (*E. coli* and MRSA) were grown overnight in NB at 37 °C. After that, the secondary cultures were inoculated in new NB broth media to obtain cells in their exponential phase at 0.5–0.6 OD_{600}. *E. coli* and MRSA were pelleted down and washed with PBS three times. After washing, they were resuspended in PBS. Typically, the dye (10 μg/mL) was then mixed with the bacteria (1:1 v/v) after resuspension and incubated for 20 min. Finally, 50 μL of bacterial suspension mixed with the dye was dropped on a glass slide and covered with a cover slip. After drying for a few minutes, images were taken (Olympus I × 51) at 40× magnification and captured with an Olympus DP70 camera.

2.4. Antibacterial Activity of SO_3SQ Against Bacteria (E. coli)

The antibacterial activity of SO_3SQ was determined by double dilution of broth according to the guidelines recommended by the Clinical and Laboratory Standard Institute (CLSI, USA). [49] Briefly, in a sterile 96-well plate, 50 μL of NB and 50 μL SO_3SQ (in media) were added initially in the first row of a 96-well plate. The other subsequent wells were filled with 50 μL of media only. After that, serial dilutions were made such that each well received 50 μL of the test dye with a final concentration ranging from 3.90 to 2000 μg/mL. 5×10^6 CFU/mL of bacterial suspension was added to each well to give a total volume of 100 μL. The bacterial suspension wells with no dye added was used as a control. After that, the 96-well plate was incubated at 37 °C for 16–18 h. The visible growth of bacterial cells was estimated at OD_{600} using a 96 well-plate reader. The minimum concentration at which no visible turbidity was observed was taken as the minimum inhibitory concentration (MIC). [50–52]

$$\text{Percentage biofilm formation} = \frac{(\text{Control absorbance} - \text{sample absorbance}) \times 100}{\text{Control absorbance}}$$

2.5. Photothermal Effect of SO_3SQ in PBS

In brief, a sterile 96 well-plate was taken in which a total volume of 100 μL of SO_3SQ in PBS with a concentration ranging from (3.90–1000 μg/mL) was irradiated for 20 min using an 808 nm wavelength laser equipped with a thermal imaging camera. The graph was plotted as temperature (°C) versus time in 30 s intervals from the data obtained.

2.6. Photothermal Effect of SO_3SQ Against Bacteria

The bacterial strains were cultured in NB and cell concentrations up to 10^8 CFU/mL were maintained. [50] To check the effect of PTT on bacterial viability, different concentrations of dye ranging from 62.5 to 2000 μg/mL were added to 5×10^5 CFU/mL bacterial strains cultures and irradiated with NIR light for 20 min using an 808 nm wavelength laser equipped with a thermal imaging camera in the 96-well plate. After irradiation, the bacteria were sampled, cultured, and incubated for 16–18 h on Nutrient Agar (NA) plates. After 16 h, the bacteria colony number was counted using a colony count reader. The irradiated bacterial samples without dye were taken as a control.

2.7. Live/Dead Imaging

Cell viability (live/dead staining) of bacteria killed after treatment with SO_3SQ under NIR radiation was assessed. [53] For this, in 100 mL of PBS, a fluorescent dye solution containing 100 μg of acridine orange and 100 μg of ethidium bromide was mixed and prepared. In a sterile 96-well plate, 50 μL of NB and 50 μL SO_3SQ (in media) were added and mixed. After that, a two-fold dilution was made, and finally, 5×10^6 CFU/mL of the bacterial suspension was added to each well to reach a total volume of 100 μL. The samples were then irradiated with NIR light for 20 min using an 808 nm wavelength laser equipped with a thermal imaging camera. After irradiation, the cultures were mixed with 100 μL of prepared fluorescent dye solution and incubated for 15 min. The excess dye was removed by washing twice with PBS for 15 min. Lastly, the cells were observed under a fluorescence microscope (Olympus IX51) at 40× magnification, and captured images were obtained with an Olympus DP70 camera. Controls without SO_3SQ were subjected to the same NIR irradiation with an equal volume of the media.

2.8. Biofilm Inhibition Assay

The inhibitory effect of SO_3SQ on biofilm formation was investigated using the crystal violet assay. [51] The bacterial cultures were maintained in NB. The cell culture was maintained at an average of 10^8 CFU/mL, and 50 μL of culture was added to a 96-well plate containing 50 μL of SO_3SQ solution at various concentrations ranging from 500 to 2000 μg/mL by serial double dilutions. The samples were then irradiated with an 808 nm NIR laser equipped with a thermal imaging camera for 20 min, followed by incubation of the 96-well plate for 24 h at 37 °C. After 24 h, the free-floating planktonic cells were removed by washing three-time with PBS, and then 0.1% (100 μL) of the crystal violet solution was added to each well and incubated for 20 min. The crystalline violet solution was then removed and washed three times with sterile PBS to remove excess stains. [50–52] The dye was then dissolved in 100 μL of ethanol, and the OD_{595} nm was recorded. The percentage of biofilm inhibition was calculated as follows:

2.9. Photothermal Effect of SO_3SQ on Preformed Young and Mature Biofilms

To check the biofilm-eradication behavior and to analyse the mature biofilm eradication concentration (MBEC) of SO_3SQ under NIR irradiation, biofilms were grown and formed in a 96-well plate by inoculating 10^8 CFU/mL bacterial cells at 37 °C for 6 h to form young biofilms and for 24 h to form mature biofilms. [50–52] After biofilm formation, planktonic cells were washed out with sterile PBS. Then, 100 μL of SO_3SQ solution (concentration ranging from 500 to 2000 μg/mL) was added to each well, followed by irradiation for 20 min with an 808 nm NIR laser equipped with a thermal imaging camera. After irradiation, the 96-well plates were incubated at 37 °C for 24 h. After 24 h, a crystal-violet assay was performed, as described in the previous section.

2.10. Imaging of Bacterial Biofilms using Fluorescence Microscopy

Biofilm formation was assessed by staining live/dead bacteria in biofilms using double staining with AO and EB dyes (100 μg/mL) in the dark for 15 min, as previously described in the above experimental section.

3. Results and Discussion

In this study, all the experiments were performed in phosphate-buffered saline (PBS) solvent. The absorption and fluorescence properties of SO_3SQ in PBS solution are studied. The UV–Vis–NIR absorbance of the SO_3SQ in PBS solution at various concentrations is shown in Fig. 1 (a). The dye exhibits higher energy absorption features extending between 590 and 780 nm with two absorption peaks at 650 nm and 700 nm. A lower energy absorbance is also observed at 880 nm, which is likely due to aggregate formation. Aggregation in aqueous solution has been reported for other squaraine dyes with sulfonate groups. [43,44] This hypothesis is supported by the fact that as the concentration of SO_3SQ increases, the ratio between the higher energy features and the lower energy features changes dramatically. Under dilute conditions (Fig. S2), the higher energy portion (~600–750 nm) of the observed absorption profiles in PBS solvent are similar to the previous report for SO_3SQ in H_2O, DMSO, and MeOH. [48] As the concentration of the dye increases, the higher energy features broaden, and the lower energy absorption feature in the NIR predominates the absorption spectrum.

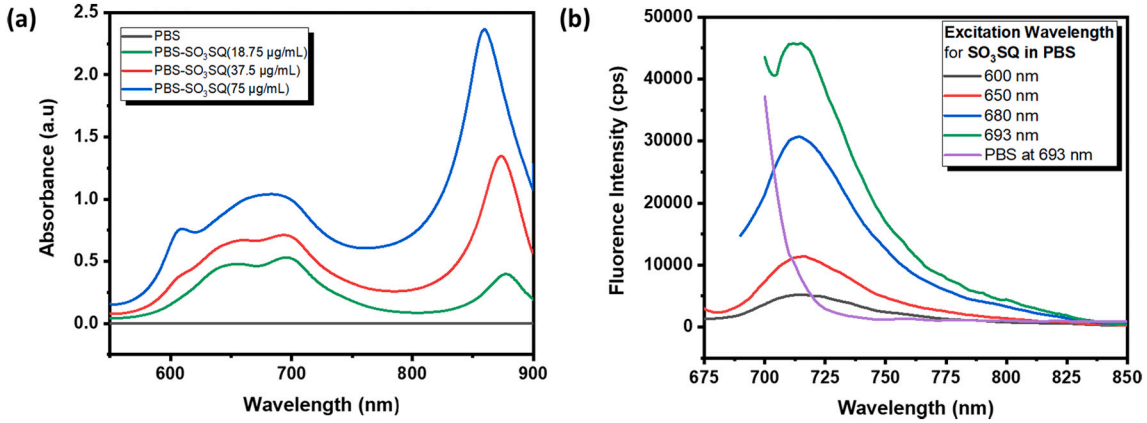

Fig. 1. (a) UV–Vis–NIR absorption of varying concentrations of SO_3SQ in PBS, (b) Fluorescence emission spectra of PBS with SO_3SQ (18.5 μg/mL) at various excitation wavelengths.

This feature could be useful for photothermal therapy as it is likely an aggregate, which tend to be naturally non-emissive. The shift in the absorption maxima to longer wavelengths places these dyes in the optimal range for in vivo PTT applications. The aggregates in PBS could be H-aggregate or J-aggregate in nature with suggested structures shown in Fig. S3. H- and J-aggregates are common aggregation modes for chromophores, including squaraines. [54,55] The pronounced shoulder peak at 650 nm is indicative of H-aggregates, and the absorption peak near 875 nm is indicative of J-aggregates based on spectral shifts only.

To further explore the possibility of aggregation in an aqueous solution, the ^{1}H NMR spectrum of SO_3SQ in an aqueous solution (D_2O) was compared to the ^{1}H NMR in an organic solvent (DMSO-d_6, Fig. S4). The ^{1}H NMR can be used to monitor aggregation since aggregates alter the local chemical environment and mobility of molecules. These changes can influence chemical shifts, peak broadening, as well as the shape and intensity of the signals. [56] The ^{1}H NMR spectrum of SO_3SQ in DMSO-d_6 exhibits chemical shifts and peak splitting similar to what was observed in CD_3OD-d_4. [48] The ^{1}H NMR spectrum of SO_3SQ in D_2O exhibits broadened signals for all hydrogens and a significant change in the chemical shifts. The *J* coupling could no longer be identified due to the broadening of the signals. The ^{1}H NMR spectra indicate that the dye molecules could not move as freely in an aqueous solution as in DMSO-d_6. Confirming an aggregate structure is challenging though, and realizing the geometry of the aggregate would require further evaluation through additional experiments in the future.

Fig. 1 (b) shows the fluorescence spectra of SO_3SQ (18 μg/mL) in PBS with different excitation wavelengths of 600 nm, 650 nm, 680 nm, and 693 nm. The emission maxima is observed at 712 nm for all excitation wavelengths, indicating that the same emissive species is responsible for the observed emission spectrum. With increasing excitation wavelengths ranging from 600 nm to 693 nm, the intensity of the fluorescence emission at the wavelength of 712 nm increases. This is because the absorption maxima of the monomeric SO_3SQ in PBS solution is near 700 nm. Exciting toward the absorption maxima increases the amount of light absorbed and generates a more intense emission spectrum. Excitation in the 800–840 nm range yielded no fluorescence emission, as shown in Fig. S5, further indicating that the aggregate species may be utilized for PTT.

The fluorescence of SO_3SQ was then studied in the presence of *E. coli* bacteria at a concentration of 10^7 CFU/mL. The solutions were incubated with different dye concentrations for 20 min. After that, the fluorescence spectra were measured at 693 nm (Fig. 2 (a)). With the addition of SO_3SQ, the intensity of the fluorescence emission at 712 nm increases. As a comparison, fluorescence spectra at excitation wavelengths of 650 nm (Fig. S6(a)) and 680 nm (Fig. S6(b)) were studied. It was observed once again that 693 nm wavelength excitation gives a higher fluorescence intensity compared to 650 nm and 680 nm wavelength excitation.

The fluorescence intensity of SO_3SQ was also monitored with constant dye concentration and different concentrations of *E. coli* ranging from 10^1 to 10^8 CFU/mL under excitation with a 693 nm laser. The fluorescence intensity was observed to increase as the concentration of bacteria increased (Fig. 2 (b)). No fluorescence was observed in the

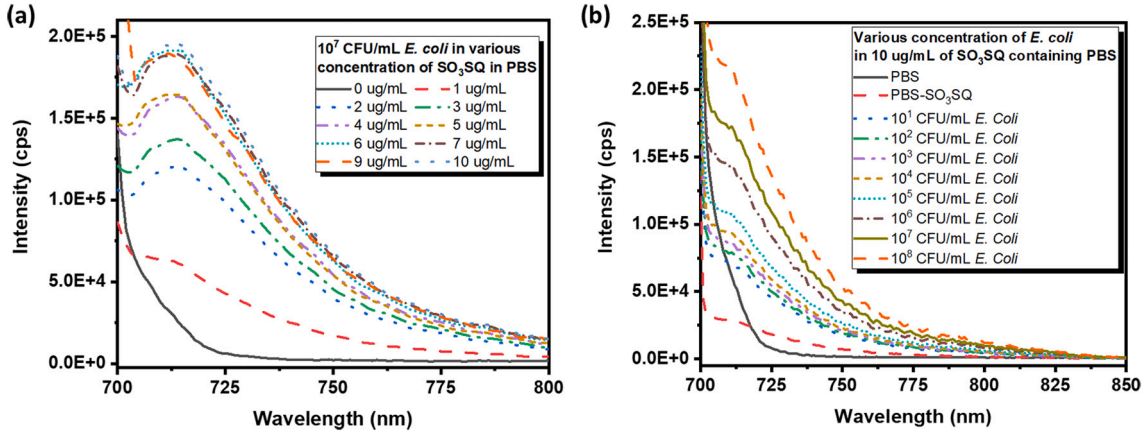

Fig. 2. (a) Fluorescence spectra of 10^7 CFU/mL *E. coli* in PBS with varying concentrations of SO_3SQ using 693 nm excitation wavelength. (b) Fluorescence spectra of 10^1–10^7 CFU/mL *E. coli* in PBS with SO_3SQ at 693 nm excitation wavelength.

E. coli solution without dye (Fig. S6 (c)). This result demonstrates that SO_3SQ exhibits a turn-on fluorescence mechanism upon interacting with *E. coli*. This unique fluorescent property is useful for bacterial imaging as the turn-on fluorescence mechanism avoids the need for washing after staining since the free dye provides minimal signal.

3.1. Bacterial Imaging using SO_3SQ

Applications using the increase in fluorescence emission of SO_3SQ upon targeting Gram-positive and Gram-negative bacterial strains were verified by conducting in-vitro fluorescence microscopy experiments using SO_3SQ with planktonic cultures of MRSA and *E. coli*. First, a ~ 10^7 CFU/mL bacterial sample was stained with SO_3SQ in PBS buffer for 20 min to bind the dye with the bacteria. After SO_3SQ treatment, bacterial cells were directly used for fluorescence microscopy imaging without washing. SO_3SQ was observed to bind with both the Gram-positive and Gram-negative bacteria, giving fluorescence as shown in Figs. 3 (a) and (b), respectively. As expected, strong fluorescent staining was observed for both genera, although Gram-negative strains tended to show less staining, indicating either a weaker interaction with the surface of the Gram-negative bacteria cells or an interaction that does not promote radiative pathways. As a control for the imaging, MRSA was incubated without SO_3SQ and demonstrated no fluorescence, as shown in Fig. 3 (c). SO_3SQ was also observed to exhibit little to no detectable fluorescence without bacteria present under the same excitation wavelength as shown in Fig. S7. The targeting mechanism of SO_3SQ binding to the bacteria is likely hydrophobic in nature, with the hydrophobic core of SO_3SQ preferentially interacting with the hydrophobic components of the bacterial cell membrane. Specifically, SO_3SQ could interact with the amphipathic lipopolysaccharide (LPS) for Gram-negative bacteria and peptidoglycans for Gram-positive bacteria. [57,58]

3.2. Antibacterial Activity of SO_3SQ Against Bacteria

Biocompatibility is a concern with any dye used in biology. Most natural and synthetic dyes currently used for microbial fluorescent staining are toxic or carcinogenic and are harmful to animals, humans, and the environment. [59–61] To check the toxicity of the SO_3SQ against pathogens, we used the broth double dilution method against *E. coli* and MRSA with different concentrations of SO_3SQ without irradiation. [49] As given in supplementary data (Fig. S8), visible growth of microorganisms was observed with SO_3SQ present at concentrations ranging from 31.25 to 2000 μg/mL along with a control without dye in a 96 well-plate. Previous results suggest that SO_3SQ is not toxic to animal cells, [48] and herein it is demonstrated that the same is true for bacterial cells. This finding indicates that without NIR irradiation, SO_3SQ possesses little to no toxicity and has a high biocompatibility for bacterial imaging.

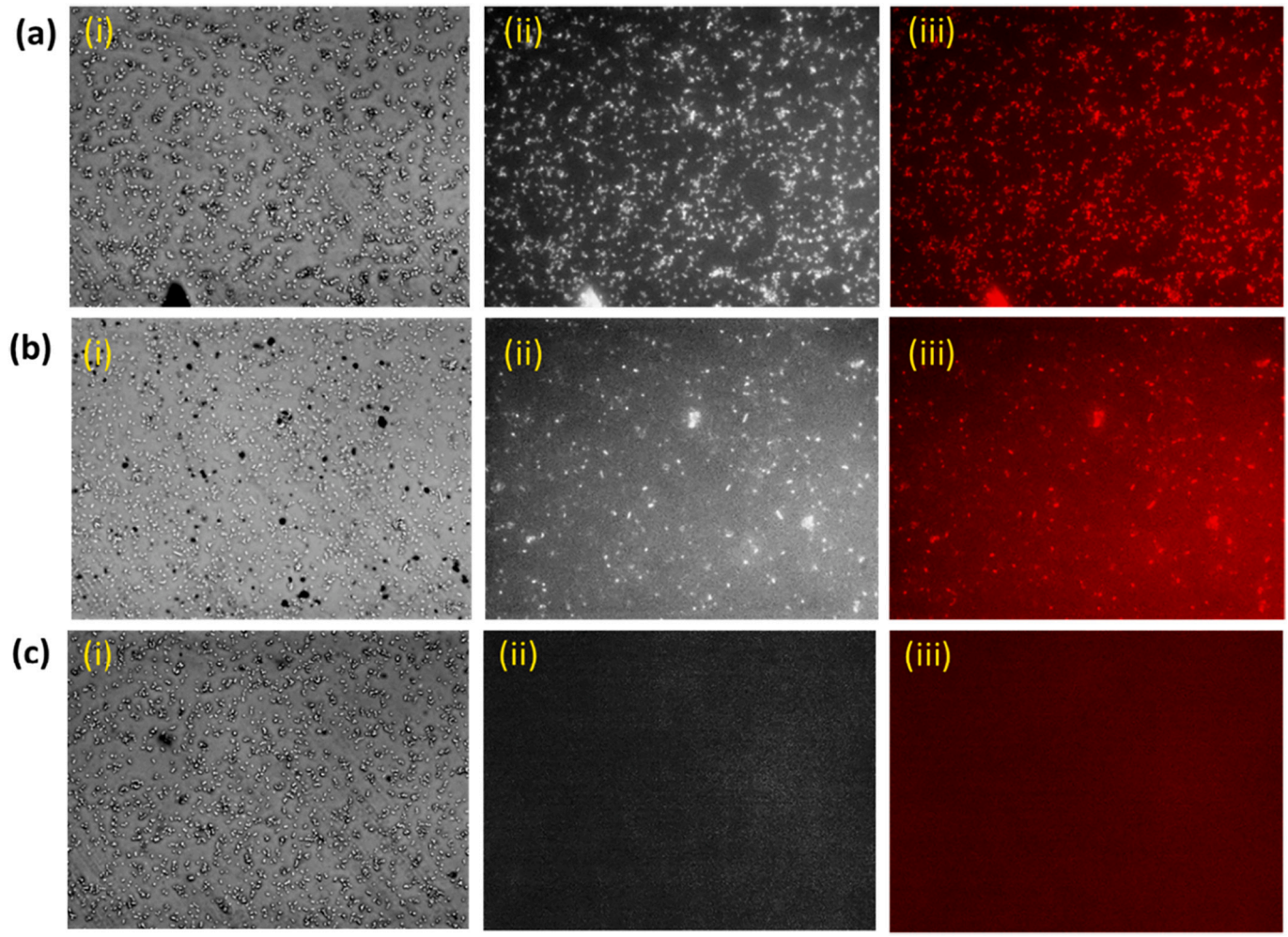

Fig. 3. Fluorescence images of MRSA and *E. coli* treated with SO_3SQ under the excitation of 604–632 nm red light. Fluorescence images of (a) MRSA and (b) *E. coli* at 10^7 CFU/mL stained with SO_3SQ. (c) Fluorescence images of MRSA at 10^7 CFU/mL in the absence of SO_3SQ (control). (i) Bright field image of bacteria, (ii) greyscale fluorescence image of bacteria, and (iii) redscale fluorescence image of bacteria. Images taken at 40× magnification. (For interpretation of the references to colour in this figure legend, the reader is referred to the web version of this article.)

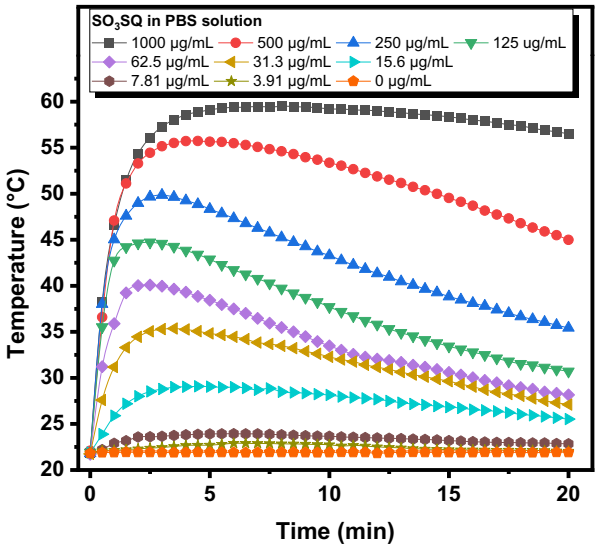

Fig. 4. Photothermal characteristics of SO_3SQ at different concentrations (0–1000 µg/mL) in PBS solution.

3.3. The Photothermal Effect of SO_3SQ in PBS

Near-infrared (NIR) light (690–1100 nm) is widely used for photothermal therapy (PTT) owing to its specific lesion therapeutic efficacy and reduced side effects on normal tissues. [25,62,63] Based on the NIR absorption exhibited by the SO_3SQ aggregate, an 808 nm laser light is selected as the excitation light source to measure photothermal effects. The photothermal conversion results of SO_3SQ in PBS at different concentrations under NIR laser irradiation over a 20-min period are shown in Fig. 4. The results indicate that the photothermal behavior is concentration-dependent. After being exposed to NIR light, the temperature of the solution undergoes a rapid (< 5 min) increase from 22 °C to 60 °C at a 1000 µg/mL dye concentration. The temperature reached by the solutions also appears to be proportional to the amount of SO_3SQ in the solution. At higher concentrations of SO_3SQ (500 µg/mL and 1000 µg/mL), the temperature reaches >55 °C, which proves that SO_3SQ has an excellent photothermal conversion efficiency. The control solution of PBS without dye shows a faint rise of 0.5–1 °C, demonstrating that SO_3SQ is imperative for the PTT effect. In each case, the maximum temperature saturation is achieved within 5 min and is observed to decrease gradually over the next 15 min, presumably due to photobleaching of the dye.

3.4. Photothermal Effect of SO_3SQ Against Bacteria

Laser irradiation-assisted photothermal therapy (PTT) converts infrared light energy into heat, which rapidly kills bacterial cells by increasing local temperature. [64,65] PTT is of interest because NIR lasers can be applied non-invasively and focused on a desired position. To date, the bactericidal efficacy of PTT is relatively low, despite numerous efforts to improve results with topical treatment of infections. [18] SO_3SQ was observed to rapidly (<5 min) generate temperatures up to 60 °C under NIR irradiation as discussed in the previous section, demonstrating excellent properties for PTT. For this reason, SO_3SQ was investigated for its ability to kill bacteria under 808 nm laser irradiation.

Bacterial cells (*E. coli* and MRSA) were incubated with SO_3SQ for 20 min, then irradiated with an 808 nm laser at a power density of 0.7 W/cm^2 for 20 min. After 20 min of irradiation, the bacterial cells were plated on agar plates and incubated for 12–16 h. The bactericidal ability of SO_3SQ was quantified by a standard plate count assay via counting the number of viable bacteria after incubation under NIR irradiation treatment. It can be seen that the number of viable bacteria decreased significantly as the dye concentration increased under NIR irradiation when compared to the non-irradiated bacterial cells with SO_3SQ and the irradiated bacterial cells without SO_3SQ as shown in Fig. 5 (a) and Fig. 6 (a) for *E. coli* and MRSA, respectively. These results confirm the exceptional bactericidal properties of SO_3SQ via the PTT effect. Temperature versus time curves for both of the bacterial strains in PBS with SO_3SQ reach temperatures >55 °C (Fig. 5 (b) and Fig. 6 (b)).

Quantitative evaluation results show that bacteria cells treated with SO_3SQ without laser irradiation remain 100% viable at each SO_3SQ concentration. However, the cell viability significantly decreased from 94.1% to 0% and 93.1% to 0% for *E. coli* and MRSA, respectively, as the SO_3SQ concentration increases from 62.5 to 2000 µg/mL with laser irradiation, as shown in Fig. 5(c) and Fig. 6 (c). From this data, it is found that concentrations ≥450 µg/mL of SO_3SQ kill over 90% of bacteria under NIR radiation. At concentrations >1000 µg/mL of SO_3SQ, 100% of bacteria are killed for both *E. coli* and MRSA. The minimum inhibitory concentration (MIC_{90}) is 450 µg/mL, presumably due to temperatures being generated above 48 °C, which irreversibly damages bacteria by destroying their proteins/enzymes and suppressing their essential intracellular reactions. [66]

3.5. Live/Dead Assay

The viability of live/dead cells for *E. coli* and MRSA was assessed using AO and EB fluorescent dyes to monitor the qualitative effect of SO_3SQ killing the bacteria using PTT. When examined under a fluorescence microscope to confirm live/dead cells, live bacterial cells appeared green and dead cells appeared red, as shown in Figs. 5 (d) and 6 (d). This is due to the differences in permeability of the two dyes in the intact/damaged membrane. The two imaging conditions, one containing SO_3SQ under NIR illumination and the other having no SO_3SQ under NIR illumination, were analyzed using ImageJ software. SO_3SQ under 808 nm laser irradiation was observed to kill nearly 100% of bacteria at higher concentrations (2000 µg/mL).

3.6. Biofilm Inhibition

Biofilms increase bacterial viability by forming an impermeable layer, generating resistance to antibiotic treatment, and eluding the host's immune response while allowing the bacteria to grow. [10] Biofilms are much more challenging to treat with antibiotics due to the limited penetration of therapeutic agents into the biofilm matrix. PTT could be one way to prevent the formation of biofilms since it does not require direct penetration of the biofilm and instead works by heating the surrounding area. For this reason, the ability of SO_3SQ to disrupt biofilm formation using PTT is evaluated using crystal violet staining.

The inhibition of several bacterial biofilms was monitored at varying concentrations of SO_3SQ under NIR light, along with the inhibition of untreated biofilms, which were monitored as controls. Concentrations of SO_3SQ ranging from 500 to 2000 µg/mL were observed to decrease *E. coli* and MRSA biofilm formation from 79% to 0% and 67% to 0%, respectively. The untreated biofilms were deemed to have 100% formation (Fig. 7 (a), (b)). The inhibition of biofilm activity is expressed via the concentration of a material that inhibits 90% of biofilm formation (BIC_{90}). BIC_{90} for SO_3SQ was determined to be >1000 µg/mL in both *E. coli* and MRSA bacterial strains. The local temperature increase induced by PTT was thus sufficient to inhibit biofilm formation by killing the bacteria present, further exemplifying the importance of the PTT effect of SO_3SQ on planktonic bacteria.

Along with biofilm inhibition, the efficacy of SO_3SQ with respect to biofilm destruction/eradication by PTT was also investigated using preformed biofilms allowed to grow for 6 h (young biofilms) and 24 h (mature biofilms) (Fig. 7 (c), (d), (e), and (f)). Under NIR irradiation, concentrations of SO_3SQ ranging from 500 to 2000 µg/mL were observed to eradicate young biofilms from a percent biofilm remaining of 86% to 2% and 83% to 1.2% for *E. coli* and MRSA, respectively. The

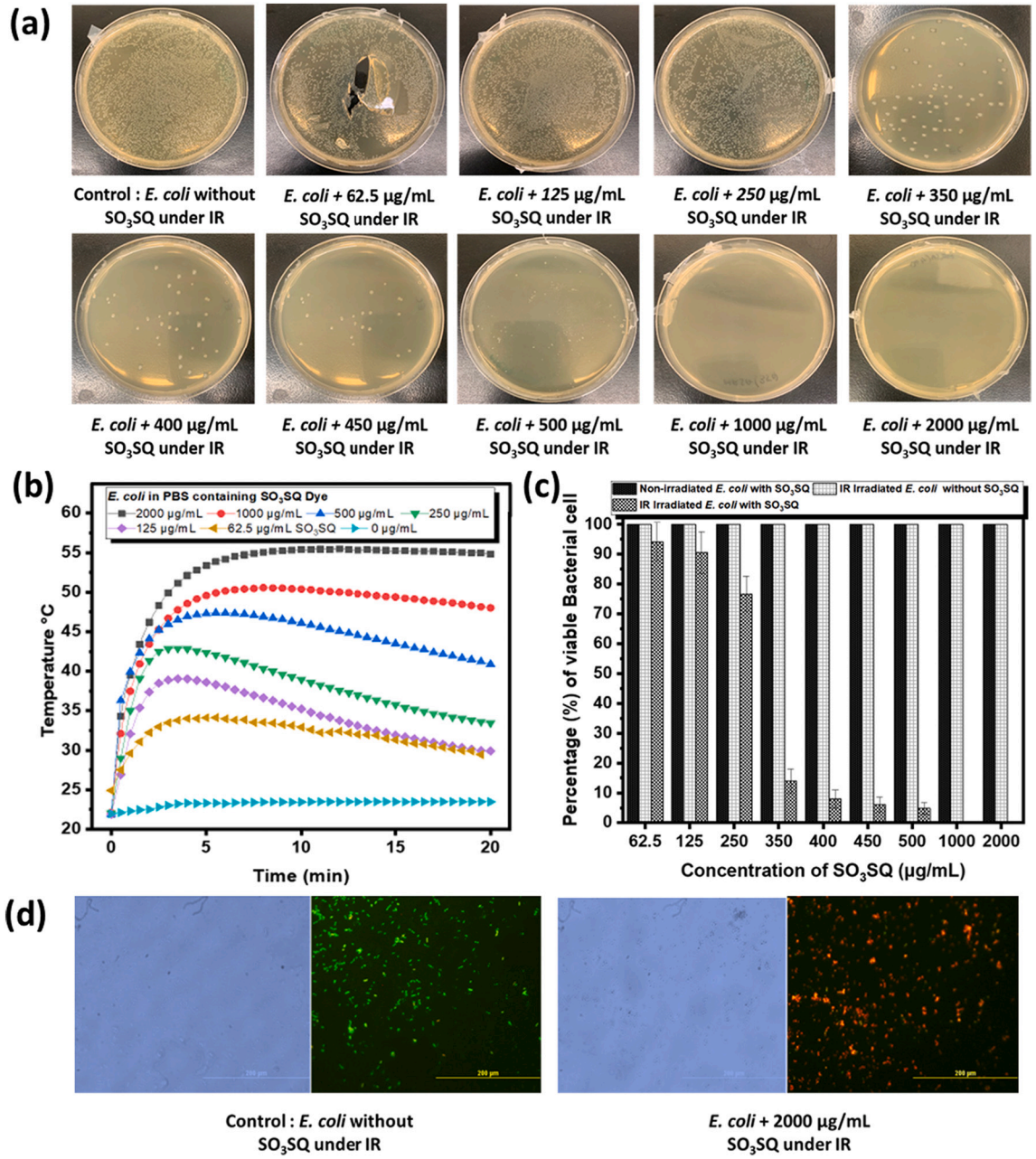

Fig. 5. The photothermal activity of SO_3SQ against *E. coli* at different concentrations ranging from 0 to 2000 µg/mL. (a) Colonies of bacteria cultured on agar plate after photothermal activity, (b) temperature vs time graph showing NIR irradiated *E. coli* with SO_3SQ in PBS, (c) percentage of viable cells remaining in different concentrations of dye after photothermal exposure. All the experiments were performed in triplicate and repeated three times. (Mean ± SD ≤ 5%). (d) Fluorescence images of bacteria treated without (left) and with (right) SO_3SQ under NIR radiation. Green cells are live cells stained with acridine orange (AO) while red cells are dead cells stained with ethidium bromide (EB). Images were taken at 40× magnification. (For interpretation of the references to colour in this figure legend, the reader is referred to the web version of this article.)

mature biofilms are eradicated from a percent biofilm remaining of 95% to 8% and 92% to 6% for *E. coli* and MRSA, respectively. In this way, the eradication of the biofilms via PTT appears to be slightly more effective at eradicating young biofilms as opposed to mature biofilms. The biofilm eradication concentration ($MBEC_{90}$) of SO_3SQ was determined to be 1500 µg/mL for young biofilms for both *E. coli* and MRSA, and 2000 µg/mL for mature biofilms for both *E. coli* and MRSA.

Biofilms grown from adhered biomasses after 6 h and 24 h showed no change in biomass from samples treated with SO_3SQ in the absence of NIR radiation. However, when the SO_3SQ treated biofilms were exposed to NIR radiation for 20 min, the bacterial biomass decreased to <10%, demonstrating that the inherent colonizing properties of bacterial biofilms were severely impaired during treatment

After treatment, the adhesive properties and characteristic morphology of the biofilm were completely destroyed. The antibiofilm activity of SO_3SQ indicates that the heat produced by NIR radiation in the presence of SO_3SQ completely disrupts the structure of the biofilm. These results suggest that SO_3SQ should have practical applications for disrupting biofilms in medical implants under NIR irradiation as has been shown previously in the literature. [65]

To verify the percentage of living bacteria in the biofilm, live/dead staining was performed. [67] It has been observed that SO_3SQ effectively inhibits biofilm formation under NIR irradiation, as shown in Fig. 8. The SO_3SQ concentration at BIC_{90} is used to prevent the

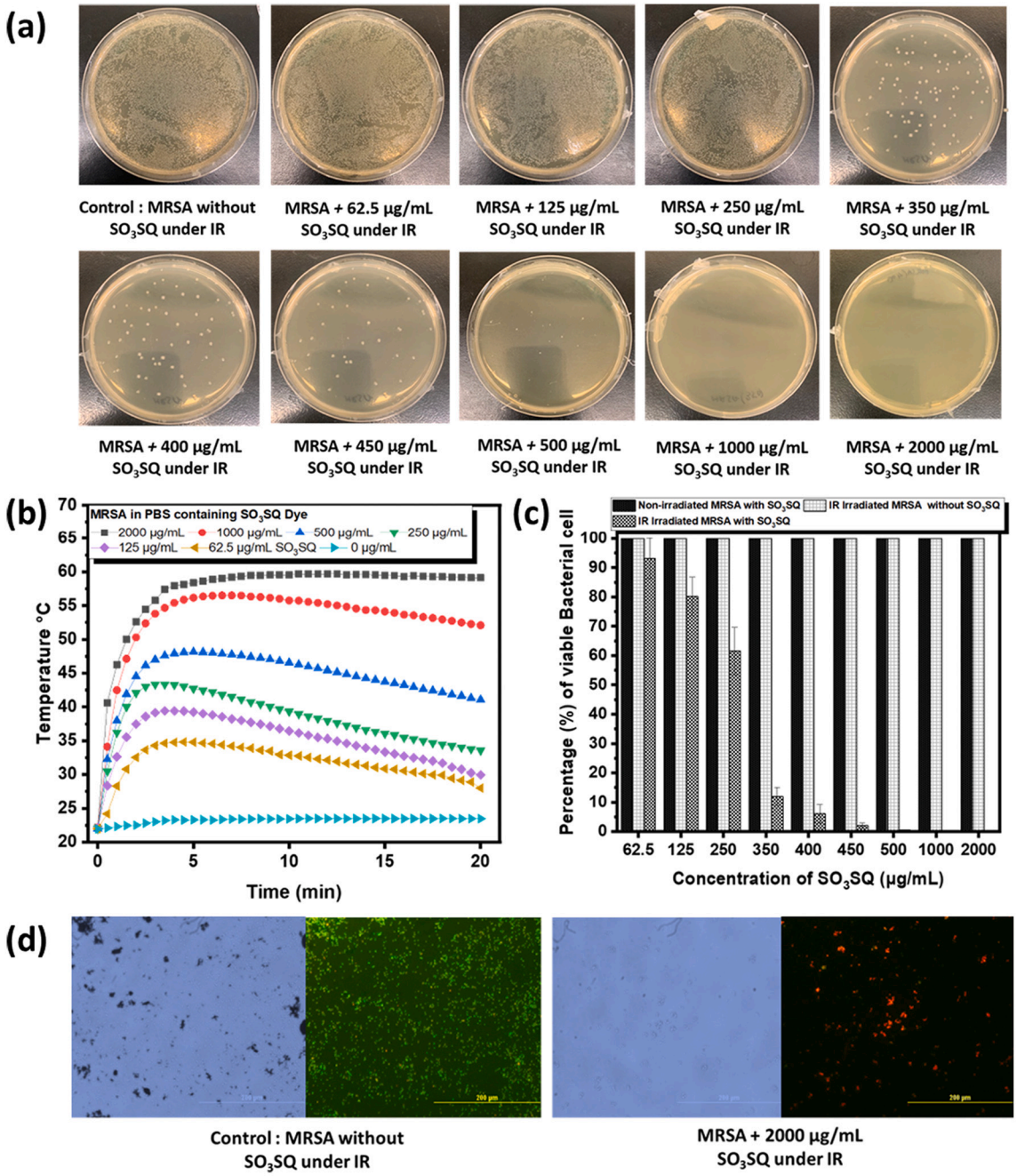

Fig. 6. The photothermal activity of SO_3SQ against MRSA at different concentrations ranging from 0 to 2000 µg/mL. (a) Colonies of bacteria cultured on agar plate after photothermal activity, (b) temperature vs time graph showing NIR irradiated MRSA with SO_3SQ in PBS, (c) percentage of viable cells remaining in different concentrations of dye after photothermal exposure. All the experiments were performed in triplicate and repeated three times. (Mean ± SD ≤ 5%). (d) Fluorescence images of bacteria treated without (left) and with (right) SO_3SQ under NIR radiation. Green cells are live cells stained with acridine orange (AO) while red cells are dead cells stained with ethidium bromide (EB). Images were taken at 40× magnification. (For interpretation of the references to colour in this figure legend, the reader is referred to the web version of this article.)

formation of biofilms in both strains. The PTT effect of NIR irradiated SO_3SQ was effective in inhibiting biofilm formation compared to control populations.

4. Conclusions

Multidrug-resistant bacteria are a severe threat to human health worldwide. Many of these bacteria often form biofilms that aid in their survival of antibiotics and facilitate the development of drug-resistant variants. This study investigates a non-toxic and biocompatible indolizine donor-based squaraine dye (SO_3SQ) for bacterial imaging and the killing of bacteria and biofilms via PTT under NIR light. The optical properties of the dye were studied in PBS. The UV–Vis–NIR absorption spectra demonstrate single monomeric behavior at low concentrations with an absorption feature at 700 nm, and aggregate-type behavior at higher concentrations with an absorption feature past 900 nm. SO_3SQ allows for the wash-free fluorescence imaging of drug-resistant bacteria via NIR fluorescence imaging due to a "turn-on" fluorescence effect of the dye when interacting with bacteria. SO_3SQ showed little to no toxicity against bacteria under non-irradiated conditions. SO_3SQ was observed to be an effective antibacterial agent via the PTT effect against both Gram-negative and Gram-positive bacteria with a MIC_{90} of >450

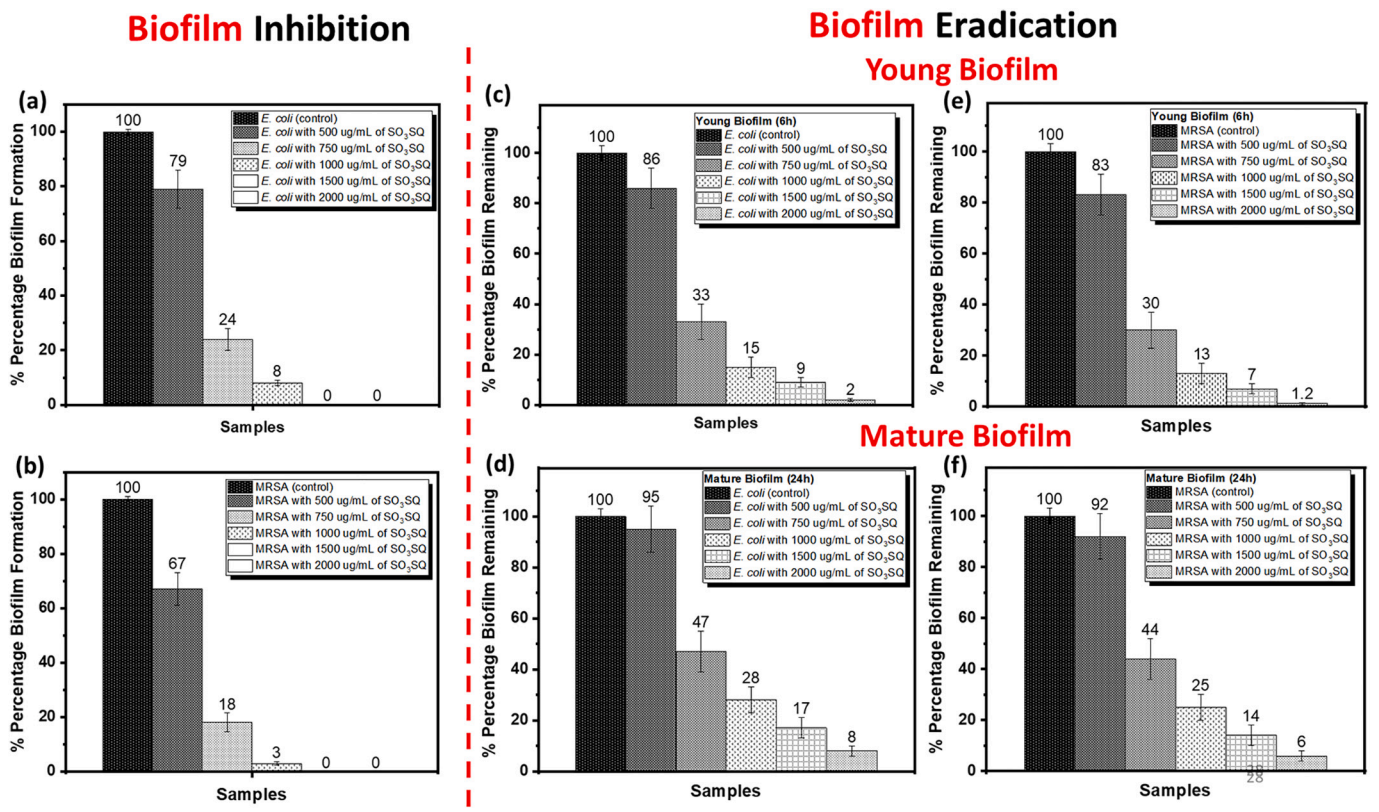

Fig. 7. Photothermal activity of SO_3SQ on biofilm formation inhibition against (a) *E. coli* and (b) MRSA was studied using a crystal violet assay and preformed on young biofilms (c) and (e) and preformed on mature biofilms (d) and (f). All the experiments were performed in triplicate and repeated three times. (Mean ± SD ≤ 5%). (For interpretation of the references to colour in this figure legend, the reader is referred to the web version of this article.)

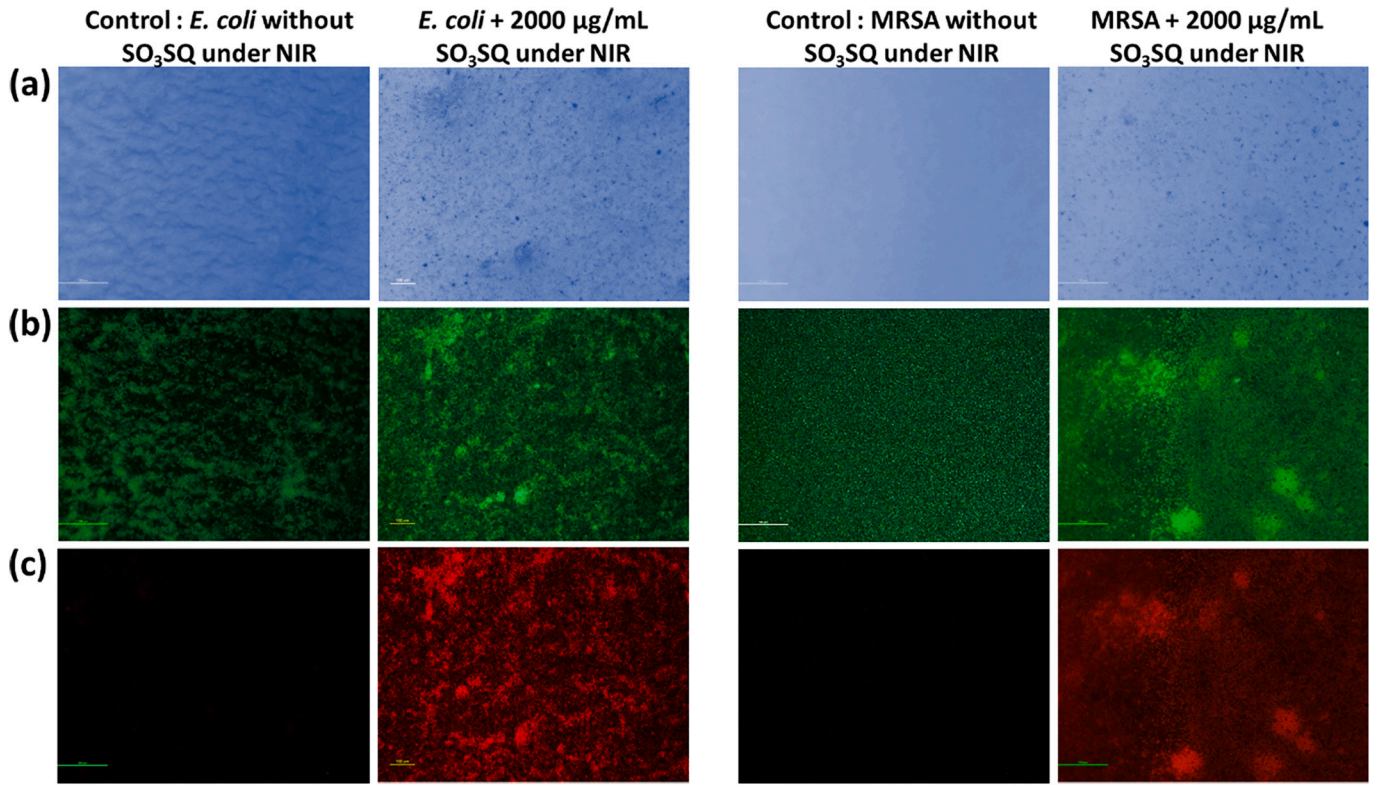

Fig. 8. Viability of bacterial cells (*E. coli* and MRSA) treated with SO_3SQ under NIR radiation in biofilms. Biofilms without SO_3SQ are used as a control. (a) Bright-field images, (b) living cells stained green with acridine orange, (c) dead cells stained red with ethidium bromide. Images taken at 40× magnification. (For interpretation of the references to colour in this figure legend, the reader is referred to the web version of this article.)

μg/mL when irradiated with a laser light of 808 nm. The PTT effect of SO_3SQ was observed to inhibit biofilm formation and eradicate both young and mature biofilms, as confirmed by live/dead imaging and crystal violet assays. These findings provide a multifunctional role for SO_3SQ in drug-resistant bacterial imaging, as well as antibacterial and antibiofilm activity for implant-related functions.

Funding Information

This research was supported by the National Science Foundation (DMR-2000135) and the National Science Foundation EPSCoR (OIA-1757220).

CRediT authorship contribution statement

Sanjay Singh: Conceptualization, Formal analysis, Investigation, Writing – original draft. **William E. Meador:** Methodology, Formal analysis, Writing – review & editing. **Avijit Pramanik:** Methodology, Resources. **Paresh Ray:** Conceptualization, Resources. **Jared H. Delcamp:** Conceptualization, Writing – review & editing. **Yongfeng Zhao:** Conceptualization, Writing – original draft, Writing – review & editing.

Declaration of Competing Interest

There are no conflicts to declare.

Data availability

Data will be made available on request.

Acknowledgements

This research was supported by the National Science Foundation (DMR-2000135) and the NSF EPSCoR (grant number: OIA-1757220).

Appendix A. Supplementary Data

Supplementary data to this article can be found online at https://doi.org/10.1016/j.jphotobiol.2023.112652.

References

[1] L. Zhang, Y. Wang, J. Wang, Y. Wang, A. Chen, C. Wang, W. Mo, Y. Li, Q. Yuan, Y. Zhang, Photon-responsive antibacterial nanoplatform for synergistic photothermal-/pharmaco-therapy of skin infection, ACS Appl. Mater. Interfaces 11 (2019) 300–310.
[2] M. Singer, C.S. Deutschman, C.W. Seymour, M. Shankar-Hari, D. Annane, M. Bauer, R. Bellomo, G.R. Bernard, J.-D. Chiche, C.M. Coopersmith, R.S. Hotchkiss, M. M. Levy, J.C. Marshall, G.S. Martin, S.M. Opal, G.D. Rubenfeld, T. van der Poll, J.-L. Vincent, D.C. Angus, The third international consensus definitions for sepsis and septic shock (Sepsis-3), JAMA 315 (2016) 801–810.
[3] K.E. Rudd, S.C. Johnson, K.M. Agesa, K.A. Shackelford, D. Tsoi, D.R. Kievlan, D. V. Colombara, K.S. Ikuta, N. Kissoon, S. Finfer, C. Fleischmann-Struzek, F. R. Machado, K.K. Reinhart, K. Rowan, C.W. Seymour, R.S. Watson, T.E. West, F. Marinho, S.I. Hay, R. Lozano, A.D. Lopez, D.C. Angus, C.J.L. Murray, M. Naghavi, Global, regional, and national sepsis incidence and mortality, 1990–2017: analysis for the global burden of disease study, Lancet 395 (2020) 200–211.
[4] M. Frieri, K. Kumar, A. Boutin, Antibiotic resistance, J. Infect. Public Health 10 (2017) 369–378.
[5] Y. Zheng, L. He, T.K. Asiamah, M. Otto, Colonization of medical devices by staphylococci, Environ. Microbiol. 20 (2018) 3141–3153.
[6] L. Crémet, A. Broquet, B. Brulin, C. Jacqueline, S. Dauvergne, R. Brion, K. Asehnoune, S. Corvec, D. Heymann, N. Caroff, Pathogenic potential of Escherichia coli clinical strains from orthopedic implant infections towards human osteoblastic cells, Pathog. Dis. 73 (2015) ftv065.
[7] I. Levin-Reisman, I. Ronin, O. Gefen, I. Braniss, N. Shoresh, N.Q. Balaban, Antibiotic tolerance facilitates the evolution of resistance, Science 355 (2017) 826–830.
[8] X. Pang, Q. Xiao, Y. Cheng, E. Ren, L. Lian, Y. Zhang, H. Gao, X. Wang, W. Leung, X. Chen, G. Liu, C. Xu, Bacteria-responsive nanoliposomes as smart sonotheranostics for multidrug resistant bacterial infections, ACS Nano 13 (2019) 2427–2438.
[9] A. Rubio-Cosials, E.C. Schulz, L. Lambertsen, G. Smyshlyaev, C. Rojas-Cordova, K. Forslund, E. Karaca, A. Bebel, P. Bork, O. Barabas, Transposase-DNA complex structures reveal mechanisms for conjugative transposition of antibiotic resistance, Cell 173 (2018) 208–220.e220.
[10] E. Wistrand-Yuen, M. Knopp, K. Hjort, S. Koskiniemi, O.G. Berg, D.I. Andersson, Evolution of high-level resistance during low-level antibiotic exposure, Nat. Commun. 9 (2018) 1599.
[11] E. Tacconelli, E. Carrara, A. Savoldi, S. Harbarth, M. Mendelson, D.L. Monnet, C. Pulcini, G. Kahlmeter, J. Kluytmans, Y. Carmeli, M. Ouellette, K. Outterson, J. Patel, M. Cavaleri, E.M. Cox, C.R. Houchens, M.L. Grayson, P. Hansen, N. Singh, U. Theuretzbacher, N. Magrini, A.O. Aboderin, S.S. Al-Abri, N. Awang Jalil, N. Benzonana, S. Bhattacharya, A.J. Brink, F.R. Burkert, O. Cars, G. Cornaglia, O. J. Dyar, A.W. Friedrich, A.C. Gales, S. Gandra, C.G. Giske, D.A. Goff, H. Goossens, T. Gottlieb, M. Guzman Blanco, W. Hryniewicz, D. Kattula, T. Jinks, S.S. Kanj, L. Kerr, M.-P. Kieny, Y.S. Kim, R.S. Kozlov, J. Labarca, R. Laxminarayan, K. Leder, L. Leibovici, G. Levy-Hara, J. Littman, S. Malhotra-Kumar, V. Manchanda, L. Moja, B. Ndoye, A. Pan, D.L. Paterson, M. Paul, H. Qiu, P. Ramon-Pardo, J. Rodríguez-Baño, M. Sanguinetti, S. Sengupta, M. Sharland, M. Si-Mehand, L.L. Silver, W. Song, M. Steinbakk, J. Thomsen, G.E. Thwaites, J.W.M. van der Meer, N. Van Kinh, S. Vega, M.V. Villegas, A. Wechsler-Fördös, H.F.L. Wertheim, E. Wesangula, N. Woodford, F.O. Yilmaz, A. Zorzet, Discovery, research, and development of new antibiotics: the WHO priority list of antibiotic-resistant bacteria and tuberculosis, Lancet Infect. Dis. 18 (2018) 318–327.
[12] Antibiotic Resistance Threats in the United States, Centers for Disease Control and Prevention, 2013. https://www.cdc.gov/drugresistance/pdf/ar-threats-2013-508.pdf.
[13] V. Velusamy, K. Arshak, O. Korostynska, K. Oliwa, C. Adley, An overview of foodborne pathogen detection: in the perspective of biosensors, Biotechnol. Adv. 28 (2010) 232–254.
[14] Y. Huang, W. Chen, J. Chung, J. Yin, J. Yoon, Recent progress in fluorescent probes for bacteria, Chem. Soc. Rev. 50 (2021) 7725–7744.
[15] J.W. Yoon, S. Kim, Y. Yoon, M.H. Lee, A resorufin-based fluorescent turn-on probe responsive to nitroreductase activity and its application to bacterial detection, Dyes Pigments 171 (2019), 107779.
[16] B. Li, Q. Yu, Y. Duan, Fluorescent labels in biosensors for pathogen detection, Crit. Rev. Biotechnol. 35 (2015) 82–93.
[17] A.P. Marshall, J.D. Shirley, E.E. Carlson, Enzyme-targeted fluorescent small-molecule probes for bacterial imaging, Curr. Opin. Chem. Biol. 57 (2020) 155–165.
[18] S. Pramanik, S.K.E. Hill, B. Zhi, N.V. Hudson-Smith, J.J. Wu, J.N. White, E. A. McIntire, V.S.S.K. Kondeti, A.L. Lee, P.J. Bruggeman, U.R. Kortshagen, C. L. Haynes, Comparative toxicity assessment of novel Si quantum dots and their traditional Cd-based counterparts using bacteria models Shewanella oneidensis and Bacillus subtilis, Environ. Sci. Nano 5 (2018) 1890–1901.
[19] L. Feng, W. Chen, X. Ma, S.H. Liu, J. Yin, Near-infrared heptamethine cyanines (Cy7): from structure, property to application, Org. Biomol. Chem. 18 (2020) 9385–9397.
[20] D. Li, W. Chen, S.H. Liu, X. Chen, J. Yin, The regulation of biothiol-responsive performance and bioimaging application of benzo[c][1,2,5]oxadiazole dyes, Chin. Chem. Lett. 31 (2020) 2891–2896.
[21] X. Han, D. Li, X. Ma, S.H. Liu, J. Yin, Photoactivatable fluorescence enhanced behaviour of benzo[c][1,2,5]oxadiazole-dressing tetraphenylethene, New J. Chem. 42 (2018) 6609–6612.
[22] L. Li, Y. Chen, W. Chen, Y. Tan, H. Chen, J. Yin, Photodynamic therapy based on organic small molecular fluorescent dyes, Chin. Chem. Lett. 30 (2019) 1689–1703.
[23] K. Deng, C. Li, S. Huang, B. Xing, D. Jin, Q. Zeng, Z. Hou, J. Lin, Recent progress in near infrared light triggered photodynamic therapy, Small 13 (2017) 1702299.
[24] S. Wang, Y. Huang, X. Guan, Fluorescent probes for live cell thiol detection, Molecules 26 (2021).
[25] J.L. Kolanowski, F. Liu, E.J. New, Fluorescent probes for the simultaneous detection of multiple analytes in biology, Chem. Soc. Rev. 47 (2018) 195–208.
[26] D.A. Jose, R. Sakla, N. Sharma, S. Gadiyaram, R. Kaushik, A. Ghosh, Sensing and bioimaging of the gaseous signaling molecule hydrogen sulfide by near-infrared fluorescent probes, ACS Sensors 5 (2020) 3365–3391.
[27] X. Du, W. Wang, C. Wu, B. Jia, W. Li, L. Qiu, P. Jiang, J. Wang, Y.-Q. Li, Enzyme-responsive turn-on nanoprobes for in situ fluorescence imaging and localized photothermal treatment of multidrug-resistant bacterial infections, J. Mater. Chem. B 8 (2020) 7403–7412.
[28] W. Chyan, R.T. Raines, Enzyme-activated fluorogenic probes for live-cell and in vivo imaging, ACS Chem. Biol. 13 (2018) 1810–1823.
[29] D. Hu, L. Zou, B. Li, M. Hu, W. Ye, J. Ji, Photothermal killing of methicillin-resistant Staphylococcus aureus by bacteria-targeted polydopamine nanoparticles with nano-localized hyperpyrexia, ACS Biomater. Sci. Eng. 5 (2019) 5169–5179.
[30] X. Li, J.F. Lovell, J. Yoon, X. Chen, Clinical development and potential of photothermal and photodynamic therapies for cancer, Nat. Rev. Clin. Oncol. 17 (2020) 657–674.
[31] M. Ramasamy, S.S. Lee, D.K. Yi, K. Kim, Magnetic, optical gold nanorods for recyclable photothermal ablation of bacteria, J. Mater. Chem. B 2 (2014) 981–988.
[32] K.B. Ayaz Ahmed, V. Anbazhagan, Synthesis of copper sulfide nanoparticles and evaluation of in vitro antibacterial activity and in vivo therapeutic effect in bacteria-infected zebrafish, RSC Adv. 7 (2017) 36644–36652.
[33] Y. Chen, W. Wu, Z. Xu, C. Jiang, S. Han, J. Ruan, Y. Wang, Photothermal-assisted antibacterial application of graphene oxide-Ag nanocomposites against clinically isolated multi-drug resistant *Escherichia coli*, R. Soc. Open Sci. 7 192019.[1] 2022.
[34] M. Yang, J. Deng, H. Su, S. Gu, J. Zhang, A. Zhong, F. Wu, Small organic molecule-based nanoparticles with red/near-infrared aggregation-induced emission for

bioimaging and PDT/PTT synergistic therapy, Mater. Chem. Front. 5 (2021) 406–417.
[35] M. Yang, Z. Özdemir, H. Kim, S. Nah, E. Andris, X. Li, Z. Wimmer, J. Yoon, Acid-responsive nanoporphyrin evolution for near-infrared fluorescence-guided photo-ablation of biofilm, Adv. Healthcare Mater. 11 (2022) 2200529.
[36] X. Li, E.-Y. Park, Y. Kang, N. Kwon, M. Yang, S. Lee, W.J. Kim, C. Kim, J. Yoon, Supramolecular phthalocyanine assemblies for improved photoacoustic imaging and photothermal therapy, Angew. Chem. Int. Ed. 59 (2020) 8630–8634.
[37] Y. Yang, P. He, Y. Wang, H. Bai, S. Wang, J.-F. Xu, X. Zhang, Supramolecular radical anions triggered by bacteria in situ for selective photothermal therapy, Angew. Chem. Int. Ed. 56 (2017) 16239–16242.
[38] J. Peng, L. Zhao, X. Zhu, Y. Sun, W. Feng, Y. Gao, L. Wang, F. Li, Hollow silica nanoparticles loaded with hydrophobic phthalocyanine for near-infrared photodynamic and photothermal combination therapy, Biomaterials 34 (2013) 7905–7912.
[39] L. Cheng, K. Yang, Y. Li, J. Chen, C. Wang, M. Shao, S.-T. Lee, Z. Liu, Facile preparation of multifunctional upconversion nanoprobes for multimodal imaging and dual-targeted photothermal therapy, Angew. Chem. Int. Ed. 50 (2011) 7385–7390.
[40] R.A. Ponzio, L.E. Ibarra, E.E. Achilli, E. Odella, C.A. Chesta, S.R. Martínez, R. E. Palacios, Sweet light o' mine: photothermal and photodynamic inactivation of tenacious pathogens using conjugated polymers, J. Photochem. Photobiol. B Biol. 234 (2022) 112510.
[41] A. Treibs, K. Jacob, Cyclotrimethine dyes derived from squaric acid, Angew. Chem. Int. Ed. Eng. 4 (1965) 694.
[42] D. Gayathri Devi, T.R. Cibin, D. Ramaiah, A. Abraham, Bis(3,5-diiodo-2,4,6-trihydroxyphenyl)squaraine: a novel candidate in photodynamic therapy for skin cancer models in vivo, J. Photochem. Photobiol. B Biol. 92 (2008) 153–159.
[43] K.M. Shafeekh, M.S. Soumya, M.A. Rahim, A. Abraham, S. Das, Synthesis and characterization of near-infrared absorbing water soluble squaraines and study of their photodynamic effects in DLA live cells, Photochem. Photobiol. 90 (2014) 585–595.
[44] K. Umezawa, D. Citterio, K. Suzuki, Water-soluble NIR fluorescent probes based on squaraine and their application for protein labeling, Anal. Sci. 24 (2008) 213–217.
[45] R.R. Avirah, D.T. Jayaram, N. Adarsh, D. Ramaiah, Squaraine dyes in PDT: from basic design to in vivo demonstration, Org. Biomol. Chem. 10 (2012) 911–920.
[46] D. Ramaiah, I. Eckert, K.T. Arun, L. Weidenfeller, B. Epe, Squaraine dyes for photodynamic therapy: study of their cytotoxicity and genotoxicity in bacteria and mammalian cells¶‡, Photochem. Photobiol. 76 (2002) 672–677.
[47] D. Ramaiah, I. Eckert, K.T. Arun, L. Weidenfeller, B. Epe, Squaraine dyes for photodynamic therapy: mechanism of cytotoxicity and DNA damage induced by halogenated squaraine dyes plus light (>600 nm)¶, Photochem. Photobiol. 79 (2004) 99–104.
[48] W.E. Meador, S.A. Autry, R.N. Bessetti, J.N. Gayton, A.S. Flynt, N.I. Hammer, J. H. Delcamp, Water-soluble NIR absorbing and emitting indolizine cyanine and indolizine squaraine dyes for biological imaging, J. Org. Chem. 85 (2020) 4089–4095.
[49] Methods for Dilution Antimicrobial Susceptibility Tests for Bacteria That Grow Aerobically (M07-A8), National Committee for Clinical Laboratory Standards, CLSI, 1990.
[50] S. Singh, P. Mishra, Bacitracin and isothiocyanate functionalized silver nanoparticles for synergistic and broad spectrum antibacterial and antibiofilm activity with selective toxicity to bacteria over mammalian cells, Biomater. Adv. 133 (2022), 112649.
[51] S. Goel, P. Mishra, Thymoquinone inhibits biofilm formation and has selective antibacterial activity due to ROS generation, Appl. Microbiol. Biotechnol. 102 (2018) 1955–1967.
[52] S. Jaiswal, P. Mishra, Antimicrobial and antibiofilm activity of curcumin-silver nanoparticles with improved stability and selective toxicity to bacteria over mammalian cells, Med. Microbiol. Immunol. 207 (2018) 39–53.
[53] L. Zhao, H. Wang, K. Huo, L. Cui, W. Zhang, H. Ni, Y. Zhang, Z. Wu, P.K. Chu, Antibacterial nano-structured titania coating incorporated with silver nanoparticles, Biomaterials 32 (2011) 5706–5716.
[54] Y. Deng, W. Yuan, Z. Jia, G. Liu, H- and J-aggregation of fluorene-based chromophores, J. Phys. Chem. B 118 (2014) 14536–14545.
[55] K. Li, X. Duan, Z. Jiang, D. Ding, Y. Chen, G.-Q. Zhang, Z. Liu, J-aggregates of meso-[2.2]paracyclophanyl-BODIPY dye for NIR-II imaging, Nat. Commun. 12 (2021) 2376.
[56] J. Hjalte, S. Hossain, A. Hugerth, H. Sjögren, M. Wahlgren, P. Larsson, D. Lundberg, Aggregation behavior of structurally similar therapeutic peptides investigated by 1H NMR and all-atom molecular dynamics simulations, Mol. Pharm. 19 (2022) 904–917.
[57] A. Krasowska, K. Sigler, How microorganisms use hydrophobicity and what does this mean for human needs? Front. Cell. Infect. Microbiol. 4 (2014).
[58] M. Zhang, J. Ouyang, L. Fu, C. Xu, Y. Ge, S. Sun, X. Li, S. Lai, H. Ke, B. Yuan, K. Yang, H. Yu, L. Gao, Y. Wang, Hydrophobicity determines the bacterial killing rate of α-helical antimicrobial peptides and influences the bacterial resistance development, J. Med. Chem. 65 (2022) 14701–14720.
[59] W. Au, T.C. Hsu, Studies on the clastogenic effects of biologic stains and dyes, Environ. Mutagen. 1 (1979) 27–35.
[60] W.M. Dion, K.A. Lord, A comparison of the toxicity of certain dyestuffs to the conidia of fusarium culmorum, Ann. Appl. Biol. 31 (1944) 221–231.
[61] U. Shedbalkar, R. Dhanve, J. Jadhav, Biodegradation of triphenylmethane dye cotton blue by Penicillium ochrochloron MTCC 517, J. Hazard. Mater. 157 (2008) 472–479.
[62] L.D. Lavis, R.T. Raines, Bright ideas for chemical biology, ACS Chem. Biol. 3 (2008) 142–155.
[63] J. Fabian, H. Nakazumi, M. Matsuoka, Near-infrared absorbing dyes, Chem. Rev. 92 (1992) 1197–1226.
[64] K. Bilici, N. Atac, A. Muti, I. Baylam, O. Dogan, A. Sennaroglu, F. Can, H. Yagci Acar, Broad spectrum antibacterial photodynamic and photothermal therapy achieved with indocyanine green loaded SPIONs under near infrared irradiation, Biomater. Sci. 8 (2020) 4616–4625.
[65] D. Bagchi, V.S.S. Rathnam, P. Lemmens, I. Banerjee, S.K. Pal, NIR-light-active ZnO-based nanohybrids for bacterial biofilm treatment, ACS Omega 3 (2018) 10877–10885.
[66] A.D. Russell, Lethal effects of heat on bacterial physiology and structure, Sci. Prog. 86 (2003) 115–137.
[67] L. Mei, Z. Lu, W. Zhang, Z. Wu, X. Zhang, Y. Wang, Y. Luo, C. Li, Y. Jia, Bioconjugated nanoparticles for attachment and penetration into pathogenic bacteria, Biomaterials 34 (2013) 10328–10337.